https://doi.org/10.5194/essd-2022-77
Preprint. Discussion started: 25 February 2022

Earth System Science Data
Open Access Discussions

SEIA: a scale-selective eddy identification algorithm for the global ocean

Yikai Yang[1,2], Lili Zeng[1,3*], Qiang Wang[1]

1. State Key Laboratory of Tropical Oceanography (LTO), South China Sea Institute of Oceanology, Chinese Academy of Sciences, Guangzhou, 510301, China

2. University of Chinese Academy of Sciences, Beijing, China

3. Southern Marine Science and Engineering Guangdong Laboratory (Guangzhou), Guangzhou, China

Corresponding Author:

Dr. Lili Zeng

State Key Laboratory of Tropical Oceanography, South China Sea Institute of Oceanology, Chinese Academy of Sciences, Guangzhou, China

Tel: (86) 20- 8902-4304; Fax: (86) 20-8902-4304

Email: zenglili@scsio.ac.cn

https://doi.org/10.5194/essd-2022-77
Preprint. Discussion started: 25 February 2022

Abstract

Automatic eddy identification algorithms are crucial for global eddy research. This study presents a scale-selective eddy identification algorithm (SEIA; https://github.com/Yk-Yang/SEIA) for the global ocean based on closed sea level anomalies (SLAs) that features two improvements in the detection and tracking processes. First, the scale-selective scheme replaces the previously used threshold for defining the eddy boundary and restricts the numbers of upper and lower grid points based on the data resolution and eddy spatial scale. Under such conditions, the eddy boundary is as large as possible, while the eddy region is not overestimated. Furthermore, a novel and effective overlap scheme is used to track eddies by calculating the intersecting ratio of time-step-successive eddies. SEIA generates 278,630 anticyclonic eddies and 274,351 cyclonic eddies from AVISO's SLA dataset over a five-year period (2015-2019; https://doi.org/10.11922/sciencedb.o00035.00004; Yang et al., 2022). The global distribution of eddies, propagation speed, and eddy path characteristics in the Southern Ocean verify the validity of SEIA.

https://doi.org/10.5194/essd-2022-77
Preprint. Discussion started: 25 February 2022

1. Introduction

Mesoscale eddies generally refer to swirling signals with space scales of 50^1-50^2 km and time scales of 10^1-10^2 days in the ocean (Morrow et al., 2012; Faghmous et al., 2015). Eddies tend to trap fluid inside (Chelton et al., 2011), causing matter and energy transport (Wyrti et al., 1976). Many studies have been conducted to explore the effects of eddies on atmospheric phenomena (Chelton et al., 2004; Frenger et al., 2013) and the transport and re-distribution of heat, salt, water masses, chlorophyll and other chemical variables (Jayne et al., 2002; Volkov, 2008; Gordon et al., 2013; Dong et al., 2014; Zhang et al., 2014; Dufois et al., 2016; Yang et al., 2021).

The study of mesoscale eddies is highly reliant on the physical characteristics of the real ocean based on in situ observations. Eddy identification algorithms are constantly emerging as a result of coarse in situ observation data and the development of satellite altimeter data. The output of the algorithms allows researchers to assess the generation, development, and extinction, as well as hydrodynamic conditions and other dynamic processes, of eddies. A complete eddy identification algorithm contains the Eulerian procedure, i.e., the detection of snapshots, and the Lagrangian procedure, namely, the tracking of eddy movement. Nencioli et al. (2016) further categorized the detection into three types: physical parameter based, flow geometry based, and hybrid. The effect of eddies can be detected in the change in sea surface variables, so in this study, we divide the variable-based algorithms into three types: 1) ecology, 2) thermodynamics and 3) dynamics.

https://doi.org/10.5194/essd-2022-77
Preprint. Discussion started: 25 February 2022

The ecological method detects eddies mainly based on chlorophyll concentration (Rodriguez et al., 2003; Dong et al., 2009; Nencioli et al., 2010; He et al., 2019). Yu et al. (2011) applied such a scheme based on MODIS chlorophyll concentration products, but it had an unsatisfactory effect on anticyclonic eddies (AEs). Sea surface temperature (SST) is the key indicator for the thermodynamics method. A flexible quasi-contour tracing and clustering method was used in Zhang et al. (2015), imposing no fixed restrictions or limitations during the course of “suspected” eddy detection. Using a high-resolution SST dataset, Moschos et al. (2020) introduced the deep learning technique to eddy detection. The issue with this type of method is that the outermost threshold of temperature may be arbitrary. Sea surface salinity (SSS) is also an effective way to detect oceanic eddies, but there are few precedents due to limited datasets.

Following the third type, many algorithms use sea surface height (SSH; Chelton et al., 2011; Mason and Pascual, 2014), SLA (Faghmous et al., 2015; Li et al., 2014, 2016; Liu et al., 2016) field, streamlines derived from the flow field (Sadarjoen and Post 2000; Nencioli et al., 2010; Le Vu et al., 2018), and physical parameters (Okubo, 1970; Weiss, 1991; Doglioli et al., 2007; Souza et al., 2011; Williams et al., 2011; Petersen et al., 2013) calculated based on geometrical properties to detect and track oceanic eddies. These methods have been widely used in related studies (we cite some; Chelton et al., 2007; Chaigneau et al., 2008, 2009; Chen et al., 2011; Liu et al., 2012; Frenger et al., 2015; Li et al., 2015; Yang et al., 2019; Yang et al., 2021). Nevertheless, these approaches suffer from a variety of deficiencies and defects. Nencioli et al. (2010) noted that the smoothing algorithm used in the Okubo-Weiss method (O-W; Okubo, 1970;

https://doi.org/10.5194/essd-2022-77
Preprint. Discussion started: 25 February 2022

Weiss, 1991) might remove physical information. Lian et al. (2019) found that the O-W method tends to perform poorly in areas with a high shear current. Furthermore, a relatively low detection rate of the O-W method was shown in Xing and Yang (2020). Similar to the SST-based method, the SSH- and SLA-based methods are typically restricted by a given threshold (Li et al., 2014; Chelton et al., 2011; Faghmous et al., 2015), which might constrain the eddy shape and, more importantly, indiscriminately remove both spurious and real features (Faghmous et al., 2015). The flow-field-based winding-angle (W-A; Sadarjoen and Post, 2000) method overestimates the eddy boundary (Tao and Yang, 2020). Nencioli et al. (2010) presented a flow-field-based method with two important parameters allowing the algorithm to be applied to data with different resolutions. Indeed, preset parameters make the method flexible but subjective and not user-friendly.

No ideal eddy detection and tracking method exists. In this study, we aim to present a scale-selective eddy identification algorithm (hereafter, SEIA) that quickly outputs results. To avoid the noted parameter issue, we enhance the initial scale selection based on the space scale definition of mesoscale eddies and the resolution of the input dataset. The upper and lower limits of grid points are set to remove false eddy-like structures and to solve the given threshold problem. The dataset and methodology of SEIA are detailed in section 2. On the basis of the output from SEIA, statistical analysis is presented in section 3 to state its reliability. Finally, a summary is provided in section 4.

https://doi.org/10.5194/essd-2022-77
Preprint. Discussion started: 25 February 2022

2. Data and methodology

2.1 Satellite and topography data

The multi-mission merged daily SLA with 1/4° resolution in both latitude and longitude from the French Archiving, Validation, and Interpretation of Satellite Oceanographic Data (AVISO) project from 2015 to 2019 is utilized to detect and track eddies. In the nearshore region, the satellite data contain signal from tides and internal waves (Yuan et al., 2006), thus the dataset of land topography and ocean bathymetry ETOPO1 from NOAA is used to mask such area.

2.2 Eddy detection principles: searching, restricting and clustering

Hausmann and Czaja (2012) reported that there are near-isotropic rotating cores within eddy composites with a typical amplitude of approximately 15 cm in the region of the Gulf Stream and the Antarctic Circumpolar Current. On the basis of this acknowledgement, with SLA from AVISO, the basic principle of eddy detection is to find appropriate closed SLA contours with a single core. The streamlines of eddies approximately correspond to closed contours of SLA, so it is possible to detect eddies based on the outermost closed contour of SLA (Chelton et al., 2011). Following Krantz et al. (1999), Zhang et al. (2015) separated the contours into four types: simple open, simple closed, concentric closed and intersecting closed (Figs. 1a-d). Various algorithms consider the multi-core structure, i.e., concentric closed contour (Fig. 1c), to study the splitting and merging of eddies (Cui et al., 2019, 2020). Here, we consider

https://doi.org/10.5194/essd-2022-77
Preprint. Discussion started: 25 February 2022

only the simple contour condition with only one core (Fig. 1b): the concentric (Fig. 1c) and intersecting (Fig. 1d) closed types degrade to this type. The red lines in Figs. 1a-d indicate the possible detection boundaries of SEIA, which we call the "mononuclear-closed" principle.

For the determination of the outermost boundary of an eddy, a scale-selective scheme is utilized instead of giving a fixed threshold of SLA (detailed in (iii) below). A preset arbitrary threshold will undoubtedly result in failed or poor detection of some eddies (Fig. 1e), as eddies evolve all the time. Taking the assessment of SEIA in the northwestern Pacific as an example (Fig. 2), the specified detection processes are as follows:

(i) Searching for SLA peaks

Initially, for a snapshot, peaks (maxima or minima) of SLA are searched in a moving 3×3 grid window (Fig. 2a). A peak occurs when the value of a grid is smaller or larger than that of the 8 neighbouring grids. Faghmous et al. (2015) implemented a 5×5 neighbourhood, suggesting that a 3×3 neighbourhood might result in too many peaks by random chance. However, the peaks detected in this step are seen only as potential or suspected cores, and unqualified peaks are deleted in the following steps. Notably, due to the nearshore issue of satellite data mentioned above, SLA shallower than certain depth (50 m for SEIA) will be masked.

(ii) Searching for closed-SLA contours

https://doi.org/10.5194/essd-2022-77
Preprint. Discussion started: 25 February 2022

Due to the AVISO SLA error of approximately 0.03 m (Ponte et al., 2007), the extreme outermost value is set to ±0.025 m (either increasing or decreasing with a step of 0.02 m) to search the closed contours. SEIA is run in MATLAB, where contours are interpolated from the original data. Therefore, a self-defined function is used to trace back to the original grids of input data under the principle of the closest values. Hence, quasi-contours are actually used in this study (Fig. 2b).

(iii) Restricting the contour grid points

After step (ii), several closed contours will exist for one eddy-like structure. Therefore, how can we define the "edge" of eddies without a given threshold? A scale-selective scheme of two restrictions is applied to solve this problem. The first is the one-core policy, which allows concentric closed contours to contract and shrink into simple closed contours (Figs. 1b-d). Furthermore, initial spatial scale filtering is the next vital limitation. The size of eddies is strictly limited to the space scale of 50^1-50^2 km with an influence radius L ranging from 25 to 125 km. Viewing eddies as quasi-circles, the approximate grid points of the influence region (Fig. 2c) can be estimated as:

$$P=2\pi L/Rs+c,\ c=1 \tag{1}$$

where $2\pi L$ is the perimeter of the eddy boundary; Rs is the resolution of the input dataset; and index c is an error-compensating correction. With Rs = 0.25° (taking $1° \approx 100$ km in both longitude and latitude) of the SLA from AVISO, the lower and upper grid points are $P_{min} \approx 7.2$ and $P_{max} \approx 32.4$, respectively.

Xing and Yang (2020) proposed the concept of a below-standard eddy whose radius fell below the resolution of the data used. With $P_{min} \approx 7.2$, eddy boundaries that occupy only 7 grid points can easily be deduced as below-standard. For the 3×3 grid window used in searching for the SLA peaks, a P_{min} of 8 is much more reasonable. Additionally, assessments have been conducted in the northwestern Pacific, showing good performance with P_{min}=10. In other words, P_{min} can be preset from 8 to 10, where 8 is ideal. P_{max} can be assigned the value calculated from formula (1), for example, P_{max}=32 in this study. Then, contours with P smaller than P_{min} or greater than P_{max} will be deleted.

Indeed, there is no universal definition of an eddy boundary. However, pre-setting a given threshold of SLA is not the best choice. Here, we innovatively propose a new scheme of restricting the pixels of boundaries accompanied by a one-core policy based on the scale definition. No arbitrary values are set, and the largest influence regions as possible are detected.

(iv) Clustering the closed contours and the peaks

After the restrictions of closed contours, the qualified peaks can be screened. Those peaks without closed contours will be removed, and the rest will be "assigned" probable closed contours ($P_{min} \leq P \leq P_{max}$); thus, other eddy information, such as radius, can be obtained. Finally, all eddies are detected in a Euler manner for one snapshot (Fig. 2d).

https://doi.org/10.5194/essd-2022-77
Preprint. Discussion started: 25 February 2022

2.3 Eddy tracking scheme

The tracking process is a complicated task as eddies deform constantly. The methodologies in previous studies vary based on the connectivity algorithm (Henson and Thomas, 2008), centre-comparing based on the background current velocity (Doglioli et al., 2007; Chaigneau et al., 2008; Nencioli et al., 2010), nondimensional parameters (Penven et al., 2005; Chen et al., 2011), parameter W from the O-W method (Chelton et al., 2011) and so on. In this study, a quick and effective methodology is proposed for the first time: the overlap scheme.

For a detected eddy, the overlap scheme searches the several nearest eddies in successive time steps and calculates the ratio of intersecting area with the larger eddy region, as shown in the following formula:

$$E_s \ni \left(\frac{e_0 \cap \{e_{i,\ i=1\ldots n}\}_{<Dt}}{\max\{e_0,\ e_{i,\ i=1\ldots n}\}} \geq Rt\right) \quad (2)$$

where E_s represents a successful tracked eddy in a Lagrangian manner; e_0 is the initial eddy region and the series of e_i denotes the regions of nearest eddies; Dt is the largest searching distance of the nearest eddies; and Rt is the overlapping ratio. Eddies are determined to be the same when the ratio is larger than a certain value. Clearly, the search distance Dt and the overlapping ratio Rt are two key factors.

The determination of Dt is highly related to the nearly due west eddy propagation speed, which is essentially equal to the phase speed of long nondispersive baroclinic

https://doi.org/10.5194/essd-2022-77
Preprint. Discussion started: 25 February 2022

Rossby waves (Chelton et al., 2007; Faghmous et al., 2015). The largest phase speed of long nondispersive baroclinic Rossby waves is approximately 0.16 $m \cdot s^{-1}$ outside the equator (±10°), as reported in Chelton et al. (2007). For the daily SLA dataset, an eddy theoretically propagates approximately 13.8 km or approximately 0.14° at 30°N with an Earth radius of 6371 km. The data resolution used in this study is 0.25°, which means that movement of 0.14° cannot be captured. Therefore, the search distance Dt will be too conservative if it is set to 0.14°. However, this finding further confirms the reasonability of the overlap scheme since eddies propagate slowly. The propagation speed is usually obtained by dividing the distance of two eddy centres (either the peak or geometric centre of the boundary) by the time step. Supposing an eddy remains relatively still in two successive time steps, the change in the eddy centre is limited. The largest possible change is a shift of half of the eddy region, equal to the length of the influence radius L. In summary, the largest search distance Dt is universally set as 125 km or 1.25°. A recent study also suggested that dipole eddy pairs can travel at more than 10 times the speed of Rossby waves (Hughes and Miller, 2017), which validated the set parameter Dt.

For Rt, the derivation is much easier. Assuming a circle moves half of its diameter (Fig. 3a), the ratio of the intersecting area is approximately 0.39. However, taking the development of eddy boundaries and shapes (Chen et al., 2019) into consideration, 0.39 is too ideal for application in a real scenario. Good performance is achieved in the assessment in the northwestern Pacific with Rt=0.25, which is the recommended value on a global scale.

https://doi.org/10.5194/essd-2022-77
Preprint. Discussion started: 25 February 2022

In other words, the quick overlap scheme calculates the intersection area of two successive eddy bounds within a search distance of 1.25° to assess how relevant they are to each other. If the ratio is larger than 0.25 (including 0.25), then the eddies are considered the same eddy; otherwise, the eddies do not match and are marked as missing for one time step (Chelton et al., 2011; Liu et al., 2016).

The complete tracking logic of SEIA is illustrated in Fig. 3b. Notably, when an eddy has a state of "-tracked-missing-" in two continuous time steps, all the missing information is temporally replaced with the former tracked information and seen as a complement state, allowing the tracking procedure to continue. The eddy is considered dead with the following state of "-tracked-missing-missing-", and information will only be stored until the last "tracked" time step. For "-tracked-missing-tracked-", it means the eddy is successfully re-tracked, and the missing information, such as the bounds and centre, is interpolated from the time-neighbouring information.

3. Datasets and code availability

Based on the SLA dataset, five years (2015-2019) of SEIA's output (Yang et al., 2022) are provided without any further processing and available on the repository (https://doi.org/10.11922/sciencedb.o00035.00004). With input dataset in pre-set format, SEIA will output series of eddies as mat (MATLAB) files with incremental IDs, for example, AE_1: the first output AE marked as No.1. Table 1 displays all of the information contained in a single eddy. Specifically, the *alive* index denotes the detection state of an eddy during the tracking process outlined in Fig. 3b, which will be

https://doi.org/10.5194/essd-2022-77
Preprint. Discussion started: 25 February 2022

eliminated from the final output mat file.

The SEIA code is open-source and runs in MATLAB, allowing anyone to detect and track global eddies (https://github.com/Yk-Yang/SEIA). Regional- and global-oriented programs are both provided to address the eddy geographical boundary-crossing issue. For regional eddy identification with limited geographic range, an eddy will be marked as emerging (vanished) once it enters (exits) the regional boundary. The equator is a natural boundary since eddy generation is highly connected to the Coriolis force, over which eddy cannot cross. The land barrier makes 0° longitude a proper boundary in the north hemisphere, and the ~67° W longitude for the south hemisphere since it has the shortest distance across the sea (from Cape Horn to the Antarctic continent). That is to say, under statistical level, eddies detected by global-oriented SEIA cannot cross the ~67° W longitude in the south hemisphere. However, this setup simplifies and reduces data operation and manipulation. As a result, for global-oriented eddy identification, SLA dataset are separated into north and south hemispheres. Furthermore, regional-oriented identification is recommended for those eddy-related studies off the Cape Horn.

4. Application and validation

Given the input dataset of SLA, SEIA outputs a series of eddies with universal information of the existing time, boundary, centre and radius. As detailed in Fig. 1, all eddies of SEIA are mononuclear. However, multinuclear eddies are a key consideration in related studies (Yi et al., 2014; Li et al., 2014; Cui et al., 2019, 2020), so the multi-

https://doi.org/10.5194/essd-2022-77
Preprint. Discussion started: 25 February 2022

core structure (McS) index is added to the output of SEIA. The McS index indicates whether an eddy belongs to the same closed contour as other eddies (Table 1), which ensures that researchers can study the splitting and merging of eddies.

Executing the code on five years (from 2015 to 2019) of SLA data generates 278,630 AEs and 274,351 CEs, with a nearly 1:1 ratio. The distribution of the eddy ($\geq$10 days outside the tropics) interior occupation in each $1^{\circ}\times1^{\circ}$ square is shown in Fig. 4a. Most eddies occur in the mid-latitude and western boundary current regions, while relatively few occur at lower and higher latitudes, which is consistent with previous studies highlighting active eddy regions, such as the Gulf Stream, Kuroshio and Southern Ocean (Chelton et al., 2007; Chelton et al., 2011). Fifty percent of eddies fall in the duration span ranging from 10 to ~34 days and radius span ranging from ~22 to ~76 km (Fig. 4b). The radius gradually increases with duration for eddies globally, among which the eddies in the Pacific exhibit this relation the most, and those in the Atlantic and Indian feature larger increasing amplitudes (Fig. 5). Notably, the radius of global eddies tends to decrease when the duration exceeds approximately 220 days.

Global eddy trajectories are characteristic of a strong tendency toward westward propagation at speeds similar to the westward phase speeds of long dispersive Rossby waves (Chelton et al., 2007). Figure 4c illustrates the similar connection between the eddy westward propagation speed calculated from SEIA and the nondispersive long Rossby wave speed. Furthermore, the analysis in Ni et al. (2020) suggested that the speed of westward eddy propagation equals the speed of baroclinic Rossby waves at

https://doi.org/10.5194/essd-2022-77
Preprint. Discussion started: 25 February 2022

approximately 25°N, which separates the global ocean into a low-latitude anisotropic wavelike regime and a high-latitude isotropic turbulence regime. The results in Figure 4c indicate a turning latitude of approximately 30°N, confirming the above theory to some extent. On the other hand, eastward propagation occurs in the Kuroshio, Gulf Stream and Southern Ocean, where eddies are advected eastward by strong depth-mean flow (Chelton et al., 2011; Klocker and Marshall 2014; Ni et al., 2020). Taking the Southern Ocean as an example, nearly 18% of eddies exhibit eastward movement, unlike the dominant propagation trend in the global ocean, while only approximately 12% of eddies exhibit westward movement (Fig. 6). More long-lived eddies are active in the southern Indian part of the Southern Ocean, as detailed in Frenger et al. (2015), which again verifies the reliability and reasonability of the output from SEIA.

5. Summary

This study aims to construct a scale-selective eddy identification algorithm for the global ocean named SEIA, based on closed SLA contours, whose basic idea is that isotropic sea surface changes are regulated by eddies. SEIA includes two components, i.e., the detection and tracking process, with two improvements compared to other algorithms.

In the detection process, the standard of the determination of the eddy boundary varies in previous studies utilizing the closed contour idea. The given thresholds for the outermost contour are arbitrary and subjective. One of the two improvements of SEIA is that the given threshold is replaced by a scale-selective scheme, which provides the

https://doi.org/10.5194/essd-2022-77
Preprint. Discussion started: 25 February 2022

upper and lower limits of grid points based on data resolution and eddy spatial scale. Its essence is that the radius of the eddy cannot be smaller than the data resolution or larger than half of the spatial scale of the mesoscale under the assumption of a quasi-circle. Based on the mononuclear framework, a boundary of the eddy that is as large as possible in the span will be obtained, which is consistent with the fact that eddies continue evolving constantly. Scale-selective conditions can capture more information without overestimating the eddy region.

The second improvement of SEIA is a novel, simple but effective tracking scheme. Chelton et al. (2007) found that the propagation speed of eddies was related to the speed of long nondispersive Rossby waves, whose maximum value is approximately 0.16 m/s outside the tropics. Thus, the propagation distance of eddies is limited to daily datasets. Therefore, an overlap scheme is applied to cluster eddies in two successive time steps into the same eddy by calculating the intersecting ratio of eddy regions. Assessment of the scheme in the northwestern Pacific indicates good performance, with successful adaptation to various complex dynamic environments. Five years of eddy product and source code of SEIA are available and accessible for anyone without restriction.

The analysis of the output from SEIA is consistent with previous studies on the global distribution of eddies, propagation speed and characteristics of eddy paths in the Southern Ocean, which confirms SEIA's reasonability and reliability. Among all the eddy identification algorithms, none can claim to be the best. SEIA is constructed to make small progress to better assist the related study of mesoscale eddies. Currently,

https://doi.org/10.5194/essd-2022-77
Preprint. Discussion started: 25 February 2022

deep machine learning is gradually being applied to the eddy identification process, and we expect to follow this approach in future research.

Author contribution

YY designed the formulation of overarching research goals and aims, developed the methodology, programmed the codes, generated the SEIA datasets and wrote the initial draft. LZ and QW verified the research protocol and supervised the research activity planning and execution. QW assisted with the analysis of the results and LZ revised the draft.

Competing interests

The authors declare that they have no conflict of interest.

Acknowledgements

This study benefited from a freely available satellite dataset produced by AVISO+ (https://www.aviso.altimetry.fr) and distributed by Copernicus Marine Service (http://marine.copernicus.eu). The ETOPO1 dataset can be obtained from NOAA (https://www.ngdc.noaa.gov/mgg/global/global.html). The construction of MATLAB-based SEIA is supported by the High Performance Computing Division at the South China Sea Institute of Oceanology.

https://doi.org/10.5194/essd-2022-77
Preprint. Discussion started: 25 February 2022

References

Chaigneau, A., Eldin, G., and Dewitte, B.: Eddy activity in the four major upwelling systems from satellite altimetry (1992-2007), Progress in Oceanography, 83, 117-123, 2009.

Chaigneau, A., Gizolme, A., and Grados, C.: Mesoscale eddies off Peru in altimeter records: Identification algorithms and eddy spatio-temporal patterns, Progress in Oceanography, 79, 106-119, 10.1016/j.pocean.2008.10.013, 2008.

Chelton, D. B., Schlax, M. G., and Samelson, R. M.: Global observations of nonlinear mesoscale eddies, Progress in Oceanography, 91, 167-216, 10.1016/j.pocean.2011.01.002, 2011.

Chelton, D. B., Schlax, M. G., Freilich, M. H., and Milliff, R. F.: Satellite measurements reveal persistent small-scale features in ocean winds, Science, 303, 978-983, 10.1126/science.1091901, 2004.

Chelton, D. B., Schlax, M. G., Samelson, R. M., and de Szoeke, R. A.: Global observations of large oceanic eddies, Geophysical Research Letters, 34, 87-101, Artn L1560610.1029/2007gl030812, 2007.

Chen, G., Han, G., and Yang, X.: On the intrinsic shape of oceanic eddies derived from satellite altimetry, Remote Sensing of Environment, 228, 75-89, 10.1016/j.rse.2019.04.011, 2019.

Chen, G. X., Hou, Y. J., Zhang, Q. L., and Chu, X. Q.: The eddy pair off eastern Vietnam: Interannual variability and impact on thermohaline structure, Continental Shelf Research, 30, 715-723, 10.1016/j.csr.2009.11.013, 2010.

https://doi.org/10.5194/essd-2022-77
Preprint. Discussion started: 25 February 2022

Cui, W., Wang, W., Zhang, J., and Yang, J.: Multicore structures and the splitting and merging of eddies in global oceans from satellite altimeter data, Ocean Science, 15, 413-430, 10.5194/os-15-413-2019, 2019.

Cui, W., Wang, W., Zhang, J., and Yang, J.: Identification and census statistics of multicore eddies based on sea surface height data in global oceans, Acta Oceanologica Sinica, 39, 41-51, 10.1007/s13131-019-1519-y, 2020.

Doglioli, A. M., Blanke, B., Speich, S., and Lapeyre, G.: Tracking coherent structures in a regional ocean model with wavelet analysis: Application to Cape Basin eddies, Journal of Geophysical Research-Oceans, 112, 10.1029/2006jc003952, 2007.

Dong, C., McWilliams, J. C., Liu, Y., and Chen, D.: Global heat and salt transports by eddy movement, Nature Communications, 5, 10.1038/ncomms4294, 2014.

Dong, C., Mavor, T., Nencioli, F., Jiang, S., Uchiyama, Y., McWilliams, J. C., Dickey, T., Ondrusek, M., Zhang, H., and Clark, D. K.: An oceanic cyclonic eddy on the lee side of Lanai Island, Hawai'i, Journal of Geophysical Research-Oceans, 114, 10.1029/2009jc005346, 2009.

Dufois, F., Hardman-Mountford, N. J., Greenwood, J., Richardson, A. J., Feng, M., and Matear, R. J.: Anticyclonic eddies are more productive than cyclonic eddies in subtropical gyres because of winter mixing, Science Advances, 2, 10.1126/sciadv.1600282, 2016.

Faghmous, J. H., Frenger, I., Yao, Y., Warmka, R., Lindell, A., and Kumar, V.: A daily global mesoscale ocean eddy dataset from satellite altimetry, Scientific Data, 2, 10.1038/sdata.2015.28, 2015.

Frenger, I., Gruber, N., Knutti, R., and Muennich, M.: Imprint of Southern Ocean eddies on winds, clouds and rainfall, Nature Geoscience, 6, 608-612, 10.1038/ngeo1863, 2013.

Frenger, I., Münnich, M., Gruber, N., and Knutti, R.: Southern Ocean eddy phenomenology, Journal of Geophysical Research: Oceans, 120, 2016.

Gaube, P., McGillicuddy, D. J., Jr., Chelton, D. B., Behrenfeld, M. J., and Strutton, P. G.: Regional variations in the influence of mesoscale eddies on near-surface chlorophyll, Journal of Geophysical Research-Oceans, 119, 8195-8220, 10.1002/2014jc010111, 2014.

Gordon, A. L. and Giulivi, C. F.: Ocean eddy freshwater flux convergence into the North Atlantic subtropics, Journal of Geophysical Research-Oceans, 119, 3327-3335, 10.1002/2013jc009596, 2014.

Hausmann, U. and Czaja, A.: The observed signature of mesoscale eddies in sea surface temperature and the associated heat transport, Deep-Sea Research Part I-Oceanographic Research Papers, 70, 60-72, 10.1016/j.dsr.2012.08.005, 2012.

He, Q., Zhan, H., Xu, J., Cai, S., Zhan, W., Zhou, L., and Zha, G.: Eddy-Induced Chlorophyll Anomalies in the Western South China Sea, Journal of Geophysical Research-Oceans, 124, 9487-9506, 10.1029/2019jc015371, 2019.

Henson, S. A. and Thomas, A. C.: A census of oceanic anticyclonic eddies in the Gulf of Alaska, Deep-Sea Research Part I-Oceanographic Research Papers, 55, 163-176, 10.1016/j.dsr.2007.11.005, 2008.

Jayne, S. R. and Marotzke, J.: The oceanic eddy heat transport, Journal of Physical Oceanography, 32, 3328-3345, 10.1175/1520-0485(2002)032<3328:Toeht>2.0.Co;2,

https://doi.org/10.5194/essd-2022-77
Preprint. Discussion started: 25 February 2022

2002.

Klocker, A. and Abernathey, R.: Global Patterns of Mesoscale Eddy Properties and Diffusivities, Journal of Physical Oceanography, 44, 1030-1046, 10.1175/jpo-d-13-0159.1, 2014.

Krantz, S. G.: Handbook of Complex Variables, Birkhäuser Boston1999.

Le Vu, B., Stegner, A., and Arsouze, T.: Angular Momentum Eddy Detection and Tracking Algorithm (AMEDA) and Its Application to Coastal Eddy Formation, Journal of Atmospheric and Oceanic Technology, 35, 739-762, 10.1175/jtech-d-17-0010.1, 2018.

Li, Q.-Y., Sun, L., and Lin, S.-F.: GEM: a dynamic tracking model for mesoscale eddies in the ocean, Ocean Science, 12, 1249-1267, 10.5194/os-12-1249-2016, 2016.

Li, Q.-Y., Sun, L., Liu, S.-S., Xian, T., and Yan, Y.-F.: A new mononuclear eddy identification method with simple splitting strategies, Remote Sensing Letters, 5, 65-72, 10.1080/2150704x.2013.872814, 2014.

Lian, Z., Sun, B. N., Wei, Z. X., Wang, Y. G., and Wang, X. Y.: Comparison of Eight Detection Algorithms for the Quantification and Characterization of Mesoscale Eddies in the South China Sea, Journal of Atmospheric and Oceanic Technology, 36, 1361-1380, 10.1175/Jtech-D-18-0201.1, 2019.

Liu, Y., Chen, G., Sun, M., Liu, S., and Tian, F.: A Parallel SLA-Based Algorithm for Global Mesoscale Eddy Identification, Journal of Atmospheric and Oceanic Technology, 33, 2743-2754, 10.1175/jtech-d-16-0033.1, 2016.

Moschos, E., Schwander, O., Stegner, A., Gallinari, P., and Ieee: DEEP-SST-EDDIES:

https://doi.org/10.5194/essd-2022-77
Preprint. Discussion started: 25 February 2022

A DEEP LEARNING FRAMEWORK TO DETECT OCEANIC EDDIES IN SEA SURFACE TEMPERATURE IMAGES, in: 2020 Ieee International Conference on Acoustics, Speech, and Signal Processing, International Conference on Acoustics Speech and Signal Processing ICASSP, 4307-4311, 2020.

Nencioli, F., Dong, C., Dickey, T., Washburn, L., and McWilliams, J. C.: A Vector Geometry-Based Eddy Detection Algorithm and Its Application to a High-Resolution Numerical Model Product and High-Frequency Radar Surface Velocities in the Southern California Bight, Journal of Atmospheric and Oceanic Technology, 27, 564-579, 10.1175/2009jtecho725.1, 2010.

Ni, Q., Zhai, X., Wang, G., and Marshall, D. P.: Random Movement of Mesoscale Eddies in the Global Ocean, Journal of Physical Oceanography, 50, 2341-2357, 10.1175/jpo-d-19-0192.1, 2020.

Okubo, A.: HORIZONTAL DISPERSION OF FLOATABLE PARTICLES IN VICINITY OF VELOCITY SINGULARITIES SUCH AS CONVERGENCES, Deep-Sea Research, 17, 445-&, 10.1016/0011-7471(70)90059-8, 1970.

Penven, P., Echevin, V., Pasapera, J., Colas, F., and Tam, J.: Average circulation, seasonal cycle, and mesoscale dynamics of the Peru Current System: A modeling approach, Journal of Geophysical Research-Oceans, 110, 10.1029/2005jc002945, 2005.

Petersen, M. R., Williams, S. J., Maltrud, M. E., Hecht, M. W., and Hamann, B.: A three-dimensional eddy census of a high-resolution global ocean simulation, Journal of Geophysical Research: Oceans, 118, 2013.

Ponte, R. M., Wunsch, C., and Stammer, D.: Spatial mapping of time-variable errors in

https://doi.org/10.5194/essd-2022-77
Preprint. Discussion started: 25 February 2022

Jason-1 and TOPEX/Poseidon sea surface height measurements, Journal of Atmospheric and Oceanic Technology, 24, 1078-1085, 10.1175/jtech2029.1, 2007.

Rodriguez, F., Varela, M., Fernandez, E., and Zapata, M.: Phytoplankton and pigment distributions in an anticyclonic slope water oceanic eddy (SWODDY) in the southern Bay of Biscay, Marine Biology, 143, 995-1011, 10.1007/s00227-003-1129-1, 2003.

Sadarjoen, I. A. and Post, F. H.: Detection, quantification, and tracking of vortices using streamline geometry, Comput Graph-Uk, 24, 333-341, Doi 10.1016/S0097-8493(00)00029-7, 2000.

Souza, J. M. A. C., Montegut, C. d. B., and Le Traon, P. Y.: Comparison between three implementations of automatic identification algorithms for the quantification and characterization of mesoscale eddies in the South Atlantic Ocean, Ocean Science, 7, 317-334, 10.5194/os-7-317-2011, 2011.

Volkov, D. L., Lee, T., and Fu, L.-L.: Eddy-induced meridional heat transport in the ocean, Geophysical Research Letters, 35, 10.1029/2008gl035490, 2008.

Weiss, J.: THE DYNAMICS OF ENSTROPHY TRANSFER IN 2-DIMENSIONAL HYDRODYNAMICS, Physica D, 48, 273-294, 10.1016/0167-2789(91)90088-q, 1991.

Williams, S., Petersen, M., Bremer, P.-T., Hecht, M., Pascucci, V., Ahrens, J., Hlawitschka, M., and Hamann, B.: Adaptive Extraction and Quantification of Geophysical Vortices, Ieee Transactions on Visualization and Computer Graphics, 17, 2088-2095, 10.1109/tvcg.2011.162, 2011.

Wu, Q. L.: Region-shrinking: A hybrid segmentation technique for isolating continuous features, the case of oceanic eddy detection, Remote Sensing of Environment, 153, 90-

https://doi.org/10.5194/essd-2022-77
Preprint. Discussion started: 25 February 2022

98, 10.1016/j.rse.2014.07.026, 2014.

Wyrtki, K., Magaard, L., and Hager, J.: EDDY ENERGY IN OCEANS, Journal of Geophysical Research-Oceans and Atmospheres, 81, 2641-2646, 10.1029/JC081i015p02641, 1976.

Xing, T. and Yang, Y.: Three mesoscale eddy detection and tracking methods: Assessment for the South China Sea, Journal of Atmospheric Oceanic Technology, 243–258, 2020.

Yang, Y., Wang, D., Wang, Q., Zeng, L., Xing, T., He, Y., Shu, Y., Chen, J., and Wang, Y.: Eddy-Induced Transport of Saline Kuroshio Water into the Northern South China Sea, Journal of Geophysical Research: Oceans, 124, 2019.

Yang, Y., Zeng, L., Wang Q.: Five years (2015-2019) of global eddy product from SEIA. (V2), Science Data Bank, https://doi.org/10.11922/sciencedb.o00035.00004, 2022.

Yi, J., Du, Y., He, Z., and Zhou, C.: Enhancing the accuracy of automatic eddy detection and the capability of recognizing the multi-core structures from maps of sea level anomaly, Ocean Science, 10, 39-48, 10.5194/os-10-39-2014, 2014.

Yuan, D., Han, W., and Hu, D.: Surface Kuroshio path in the Luzon Strait area derived from satellite remote sensing data, Journal of Geophysical Research Oceans 111.C11, 2006.

Yu, H., Kang, L., and He, M.: Research on the eddy detection method based on chlorophyll concentration distribution, IEEE, 2011.

Zhang, C., Li, H., Liu, S., Shao, L., Zhao, Z., and Liu, H.: Automatic detection of oceanic eddies in reanalyzed SST images and its application in the East China Sea,

https://doi.org/10.5194/essd-2022-77
Preprint. Discussion started: 25 February 2022

Science China-Earth Sciences, 58, 2249-2259, 10.1007/s11430-015-5101-y, 2015.

Zhang, Z., Wang, W., and Qiu, B.: Oceanic mass transport by mesoscale eddies, Science, 345, 322-324, 10.1126/science.1252418, 2014.

https://doi.org/10.5194/essd-2022-77
Preprint. Discussion started: 25 February 2022

Table 1. Information contained in a single eddy detected by the SEIA.

Term	Illustration
time	Existing dates of an eddy
bound	Scale-selective SLA contours that seen as eddy boundary
center	Peaks of SLA: maximum grid points for AE and minimum grid points for CE
radius	Mean distance between *center* and all the *bound* grid points
McS	Index indicating the state of multi-core structure: 1 means the existence of such state and 0 the opposite
alive	Temporary index indicating the state of an eddy (Exists only during program operation): 1 means successful detection of an eddy, 0 means death (ready to be output), and -1 means a successful detected eddy 'missing' in the latest time step

https://doi.org/10.5194/essd-2022-77
Preprint. Discussion started: 25 February 2022

Open Access Earth System Science Data Discussions

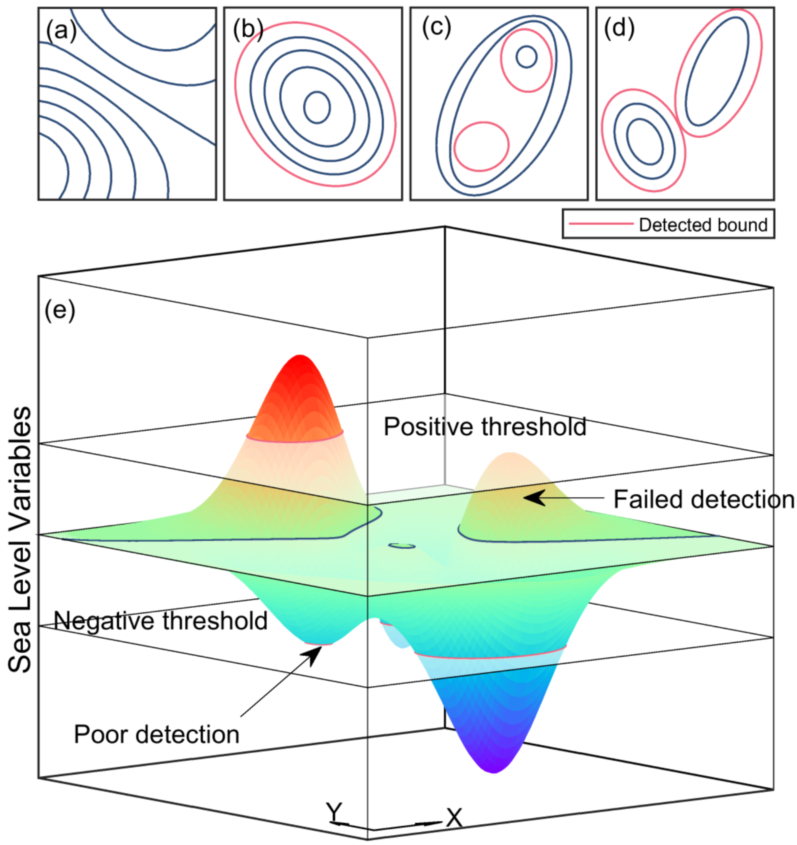

Figure 1. Contour types of (a) simple open, (b) simple closed, (c) concentric closed and (d) intersecting closed contours in Krantz et al. (1999). Red lines indicate the detected boundaries of eddies under each type; notably, the intersecting closed contours in (d) are detected as two separate eddies. (e) Diagram of eddy identification algorithms using a given threshold to determine the outermost contour or boundary of an eddy. The value of the schematic sea level variable is modified from the built-in function Peak from MATLAB 2018a.

https://doi.org/10.5194/essd-2022-77
Preprint. Discussion started: 25 February 2022

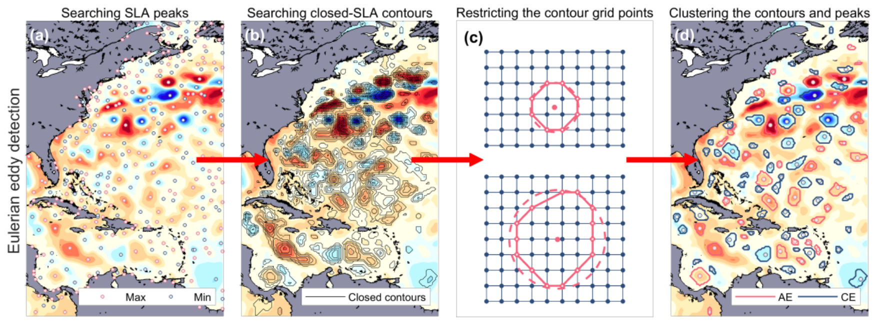

Figure 2. Four steps of Eulerian eddy detection in the northwestern Atlantic. (a) Searching for SLA peaks in a moving 3×3 grid window: red and blue dots are the maxima and the minima, respectively. (b) Searching for closed SLA contours. (c) Restricting the contour grid points based on the one-core policy and the initial spatial filtering result. (d) Clustering the closed contours with peaks into eddies.

https://doi.org/10.5194/essd-2022-77
Preprint. Discussion started: 25 February 2022

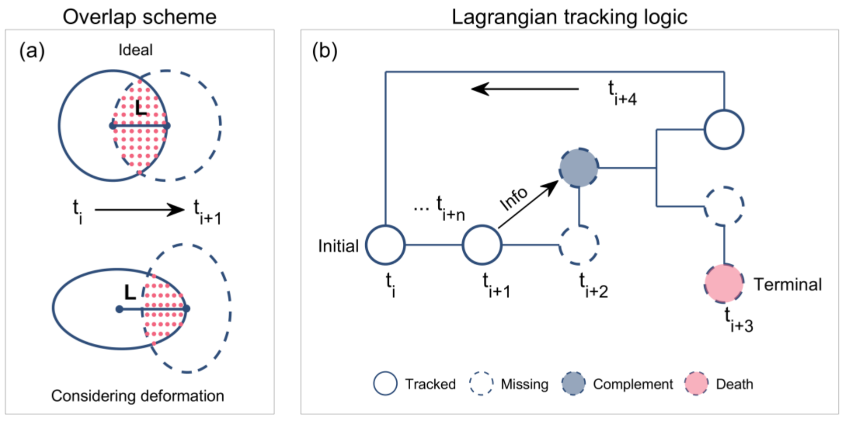

Figure 3. (a) Overlap scheme used to judge whether eddies are identical in two successive time steps. (b) Diagram of Lagrangian tracking logic: the black solid circle, black dotted circle, blue dotted circle and pink dotted circle represent successfully tracked, missing, complemental and dead eddies, respectively. The oblique arrow indicates that the missing eddy in t_{i+2} inherits eddy information from eddy in t_{i+1} to ensure the continuity of tracking, while the horizontal arrow represents a subsequent time step.

https://doi.org/10.5194/essd-2022-77
Preprint. Discussion started: 25 February 2022

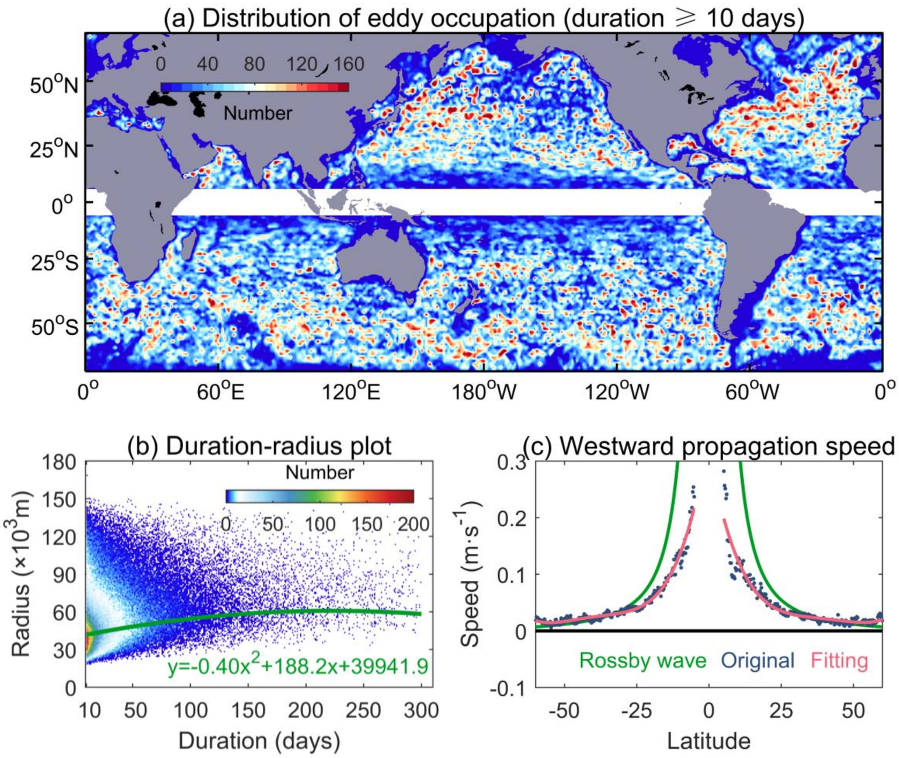

Figure 4. (a) Distribution of the eddy interior occupation in each $1^{\circ} \times 1^{\circ}$ square from 2015 to 2019. (b) Duration-radius plot of the results from SEIA in the global ocean. Colours represent certain ratios between the duration and radius; increasingly blue or red colours indicate lower or higher ratios, respectively. The green line is a quadratic fitting curve. (c) Comparison between the global eddy westward propagation speed (blue dots; m/s) and the nondispersive long Rossby wave speed (green line; m/s) evolving by latitude. The red line is the fitted curve of the original eddy westward propagation speed. Notably, only those eddies propagating westward are taken into consideration.

https://doi.org/10.5194/essd-2022-77
Preprint. Discussion started: 25 February 2022

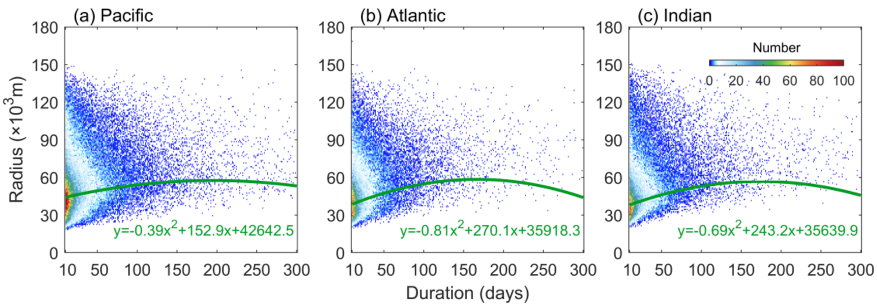

Figure 5. Duration-radius plots of the results from SEIA in the (a) Pacific, (b) Atlantic and (c) Indian Oceans. Colours represent certain ratios between the duration and radius; increasingly blue or red colours indicate lower or higher ratios, respectively. The green line is a quadratic fitting curve.

https://doi.org/10.5194/essd-2022-77
Preprint. Discussion started: 25 February 2022

Open Access Earth System Science Data Discussions

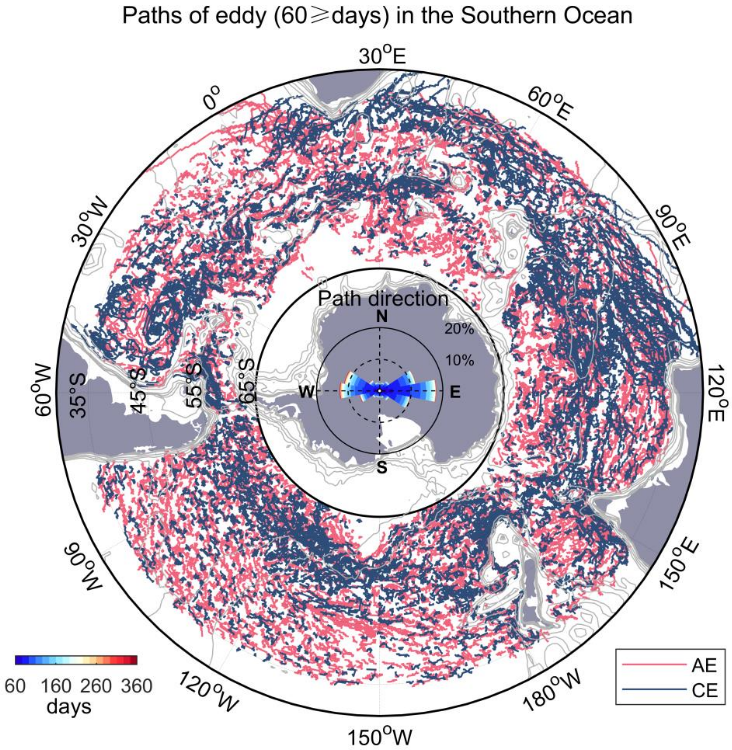

Figure 6. Paths of eddy (≥60 days) in the Southern Ocean: AEs: red lines, CEs: blue lines. The grey lines are the 3500-, 2500-, 1500-, 500-, 300-, 200- and 100- m isobaths. The eddy rose map shows the ratio of the propagation direction in 16 azimuths. The magnitude of shading indicates the lifetime of the eddy; increasingly red or blue colours represent longer or shorter lifetimes, respectively.